ELECTROCHEMISTRY

A long-life lithium-oxygen battery via a molecular quenching/mediating mechanism

Jinqiang Zhang[1]†, Yufei Zhao[1,2]†, Bing Sun[1]*, Yuan Xie[1], Anastasia Tkacheva[1], Feilong Qiu[3], Ping He[3], Haoshen Zhou[3], Kang Yan[1], Xin Guo[1], Shijian Wang[1], Andrew M. McDonagh[1], Zhangquan Peng[4]*, Jun Lu[5]*, Guoxiu Wang[1]*

The advancement of lithium-oxygen (Li-O_2) batteries has been hindered by challenges including low discharge capacity, poor energy efficiency, severe parasitic reactions, etc. We report an Li-O_2 battery operated via a new quenching/mediating mechanism that relies on the direct chemical reactions between a versatile molecule and superoxide radical/Li_2O_2. The battery exhibits a 46-fold increase in discharge capacity, a low charge overpotential of 0.7 V, and an ultralong cycle life >1400 cycles. Featuring redox-active 2,2,6,6-tetramethyl-1-piperidinyloxy moieties bridged by a quenching-active perylene diimide backbone, the tailor-designed molecule acts as a redox mediator to catalyze discharge/charge reactions and serves as a reusable superoxide quencher to chemically react with superoxide species generated during battery operation. The all-in-one molecule can simultaneously tackle issues of parasitic reactions associated with superoxide radicals, singlet oxygen, high overpotentials, and lithium corrosion. The molecular design of multifunctional additives combining various capabilities opens a new avenue for developing high-performance Li-O_2 batteries.

INTRODUCTION

Lithium-oxygen (Li-O_2) batteries have the highest theoretical specific energy among all-known battery chemistries and are deemed a disruptive technology if a practical device could be realized (*1*–*4*). Typically, a nonaqueous Li-O_2 battery consists of a lithium metal anode separated from a porous oxygen cathode by an Li^+ conducting electrolyte, and its operation relies on the stripping and plating of lithium on the negative electrode and the formation and decomposition of Li_2O_2 on the positive electrode (*5*). However, current Li-O_2 batteries suffer from challenges including low discharge capacity, poor round-trip efficiency, severe parasitic reactions, etc.

Toward solving these challenges and unlocking the energy capabilities of Li-O_2 electrochemistry, a great deal of research effort has been devoted to a fundamental understanding of the reactions and processes underpinning the operation of Li-O_2 batteries. It has been established that the discharge of an Li-O_2 battery proceeds with the oxygen reduction reaction (ORR) generating superoxide species (superoxide radicals $O_2^{\bullet-}$/lithium superoxide LiO_2) that can either adsorb on the cathode surface followed by a surface mechanism or dissolve in the electrolyte solution followed by a solution mechanism (*6*, *7*). The surface mechanism often produces Li_2O_2 with a thin layer morphology (a few nanometers in thickness) that rapidly passivates the cathode surface and leads to a low discharge capacity and a low rate capability. On the contrary, the solution mechanism usually generates Li_2O_2 with a toroidal shape (up to a few micrometers in diameter) in the electrolyte solution and can support a high discharge capacity and a high rate capability. However, toroidal-shaped Li_2O_2 is not sufficiently close to the cathode surface, and a major part of the Li_2O_2 toroid is beyond the e-tunneling range during the charge process. Therefore, the oxidation of these Li_2O_2 proceeds through mechanisms beyond simply one-step electrochemical oxidation, including direct $2e^-$ oxidation, solid-solution oxidation (via $Li_{2-x}O_2$), and stepwise oxidation (via LiO_2) (*6*, *8*–*10*). Recent studies suggest that singlet oxygen ($^1O_2$) may also be involved in discharge and charge processes, during the disproportionation reaction of LiO_2 species, and in the $1e^-$ oxidation of LiO_2 intermediates and $2e^-$ oxidation of solid Li_2O_2 (*11*). Parasitic reactions occur inevitably during both discharge and charge processes. The parasitic reactions during discharge are mainly associated with the chemical attack of battery components (electrolytes and electrodes) by the reactive oxygen species ($O_2^{\bullet-}$, LiO_2, Li_2O_2, and $^1O_2$) (*12*, *13*). However, the parasitic reactions during the charge process are more than chemical attack. Besides the chemical decomposition of battery components by reactive oxygen species generated during charging, the high voltage (>4 V) frequently applied during charging can also cause the electrochemical oxidation of the electrolyte and cathode materials, particularly in the presence of Li_2O_2 (*14*–*16*).

Many strategies have been devised to increase discharge capacity, lower charge overpotential, and alleviate parasitic reactions. These include using high donor number solvents and salts with the ability to decrease the reactivity (acidity) of Li^+, certain additives that can stabilize superoxide radicals, and redox mediators that can relay electrons between cathode surface and dissolved oxygen (*17*–*20*). These approaches have been used to promote Li_2O_2 formation in the electrolyte solution rather on the cathode surface and therefore increase the discharge capacity, among which the redox mediators demonstrate prominent performance. Nevertheless, the discharge product Li_2O_2 is difficult to be oxidized owing to its poor physical contact with the cathode surface and its intrinsically low electronic

[1]Centre for Clean Energy Technology, Faculty of Science, University of Technology Sydney, Broadway, Sydney, NSW 2007, Australia. [2]Particles and Catalysis Research Laboratory, School of Chemical Engineering, The University of New South Wales Sydney, NSW 2052, Australia. [3]Centre of Energy Storage Materials and Technology, College of Engineering and Applied Sciences, Jiangsu Key Laboratory of Artificial Functional Materials, National Laboratory of Solid-State Microstructures and Collaborative Innovation Centre of Advanced Microstructures, Nanjing University, Nanjing 210093, China. [4]Dalian Institute of Chemical Physics, Chinese Academy of Sciences, 457 Zhongshan Road, Dalian 116023, PR China. [5]Chemical Sciences and Engineering Division, Argonne National Laboratory, 9700 South Cass Avenue, Lemont, IL 60439, USA.
*Corresponding author. Email: bing.sun@uts.edu.au (B.S.); zqpeng@dicp.ac.cn (Z.P.); junlu@anl.gov (J.L.); guoxiu.wang@uts.edu.au (G.W.)
†These authors contributed equally to this work.

and ionic conductivity (*21*, *22*). Oxygen evolution reaction (OER) redox mediators have also been proposed to efficiently oxidize Li_2O_2. The oxidized form of redox mediators generated on the cathode surface can diffuse to the Li_2O_2 in the electrolyte solution and oxidize Li_2O_2 to O_2 with itself being regenerated (*23*–*30*). Because the OER redox mediators often have a redox potential that is much lower than the potential required to charge an Li-O_2 cell (usually >4.0 V), the energy efficiency of the Li-O_2 battery can be improved accordingly. Because of the low charging voltage, the decomposition of battery components during charging can be alleviated. Furthermore, to reduce the parasitic reactions caused by the attack of the reactive oxygen species, more stable electrolytes and cathode materials need to be used to construct Li-O_2 batteries (*31*–*33*). In addition, a few ORR redox mediators that can promote oxygen reduction to Li_2O_2 via a benign intermediate instead of the very reactive superoxide radicals have been used to mitigate the parasitic reactions (*19*, *34*–*40*). Similarly, molecular $^1O_2$ quencher has also been used to deactivate the reactivity of $^1O_2$, which also contributes to the suppression of overall parasitic reactions (*41*). However, the combination of these functional molecules in one cell is rarely reported. The intrinsic reactivity of each component can easily conflict with another, leading to the weakening or even deactivating of the functionalities of these individual molecules.

All in all, to realize a high discharge capacity, a low charge overpotential, and less parasitic reactions for Li-O_2 batteries, it is desirable to have a multifunctional catalyst that simultaneously has the capabilities of ORR redox mediators, OER redox mediators, and superoxide radical quencher. However, the design and synthesis of such all-in-one molecules have not been reported. Here, we rationally designed and successfully synthesized a multifunctional superoxide radical quencher by grafting two redox mediator-active 2,2,6,6-tetramethyl-1-piperidinyloxy (TEMPO) functional groups to a quenching-active perylene diimide (PDI) backbone. The as-synthesized *N*,*N*′-di-(2,2,6,6-tetramethyl-1-oxyl-4-piperidinyl)-perylene-3,4,9,10-tetracarboxylic diimide (PDI-TEMPO) molecules can not only chemically quench superoxide species generated during discharge and charge processes to suppress the generation of $^1O_2$ but also act as a redox mediator to efficiently catalyze the formation and decomposition of Li_2O_2 in the electrolyte solution and lower the discharge and charge overpotentials of Li-O_2 batteries. The synergistic effect of TEMPO and PDI moieties can also induce more functionalities to minimize parasitic reactions such as preventing the corrosion of lithium anode. When adding PDI-TEMPO in the electrolyte, the Li-O_2 batteries proceed via an alternative chemical quenching mechanism, which achieves higher discharge capacity, lower charge overpotential, less parasitic reaction, and longer cycle life.

RESULTS

Synthesis and characterization of PDI-TEMPO molecules

The PDI-TEMPO reagent was synthesized by reacting 4-amino-2,2,6,6-tetramethylpiperidine with perylene-3,4,9,10-tetracarboxylic dianhydride, followed by an oxidation process (fig. S1A), yielding reddish-purple powders as the final product (*42*, *43*). The PDI-TEMPO shows a good solubility in common electrolyte solvents used in Li-O_2 batteries, including diethylene glycol dimethyl ether (DEGDME) and dimethyl sulfoxide (DMSO) (fig. S1B). The molecular structures of PDI-TEMPO and intermediates were confirmed by several spectroscopic techniques including ultraviolet-visible (UV-Vis) spectroscopy, mass spectrometry (MS), Fourier transform infrared (FTIR) spectroscopy, and electron paramagnetic resonance (EPR) spectroscopy (fig. S2). The strong absorption bands of amide at 1650 and 1680 cm^{-1} in the FTIR spectra indicate that the TEMPO functional groups have been covalently linked to the PDI backbone (fig. S2C). Fluorescence spectroscopy shows that the TEMPO radicals in PDI-TEMPO molecules quench the fluorescence of the PDI backbones, further verifying the successful synthesis of PDI-TEMPO molecules (fig. S3) (*44*).

The PDI-TEMPO molecule features two TEMPO moieties bridged by a conjugated PDI backbone (Fig. 1A). The multifunctional PDI-TEMPO molecule is specifically designed to enhance the electrochemical performance and reduce parasitic reactions of Li-O_2 batteries (fig. S4). The conjugated PDI backbone is an efficient electron acceptor to react with $O_2^{\bullet-}$ and can behave as a quencher by quenching the reactivity of $O_2^{\bullet-}$ (*42*). The TEMPO moieties can be electrochemically reduced and oxidized and therefore can be used as a soluble redox mediator for promoting both discharge and charge reactions in Li-O_2 batteries. The chemical grafting of these moieties via chemical bonds integrates these functionalities in one molecule and enables the intermolecular interactions, which may stabilize these moieties and present individual properties without interference. The chemical bondings between these two functional moieties can not only efficiently overcome the drawback of each group (insolubility for PDI-based materials and irreversible n-doping of TEMPO molecules) but also provide additional functionalities beyond the simple combinations. These synergistic properties can also efficiently suppress the generation of $^1O_2$ (*41*, *45*, *46*). Owing to the steric interactions between the conjugated PDI backbone and bulky TEMPO moieties, PDI-TEMPO molecules have a sterically twisted structure that the TEMPO moieties and PDI backbones are not on the same plane (Fig. 1B). Such unique molecular architecture can maintain optimal van Der Waals forces via π-π interaction between the conjugated PDI backbone and the basal plane of the graphitic carbon cathode. As a result, the molecules are drawn to the surface of the carbon cathode owing to the attraction between conjugated PDI backbone and carbon cathode, while they are prevented from depositing on the cathode because of the repulsion between the bulky TEMPO moieties and carbon cathode, which prohibited its diffusion to the lithium anode (*47*).

Redox behavior of PDI-TEMPO molecules

The redox behavior of PDI-TEMPO has been examined using a glassy carbon (GC) electrode in DEGDME electrolyte. As shown in the cyclic voltammetry (CV) results in Fig. 1C, PDI-TEMPO shows three pairs of redox peaks in the voltage range of 1.8 to 4.4 V. Two pairs of redox peaks (labeled by a, a′ at ~2.8 V, and b, b′ at ~3.8 V) are assigned to the reversible reduction (a and a′) and oxidation (b and b′) of TEMPO moieties, respectively, which is consistent with previous reports (*37*, *48*, *49*). The third pair of redox peaks started at ~2.3 V originate from the electrochemistry of the PDI backbone, where the corresponding oxidation peak merges with the oxidation peak of reduced TEMPO moieties, causing the merged peak position to downshift from 3.0 V (the oxidation potential of reduced TEMPO moieties) to 2.5 V (*50*). These redox pairs are demonstrated highly reversible, showing no visible decay after three cycles (fig. S5A). Even after 25 cycles in oxygen, the characteristic redox peaks remain in the following scan in the argon atmosphere, further verifying the high stability of these redox pairs (fig. S5B).

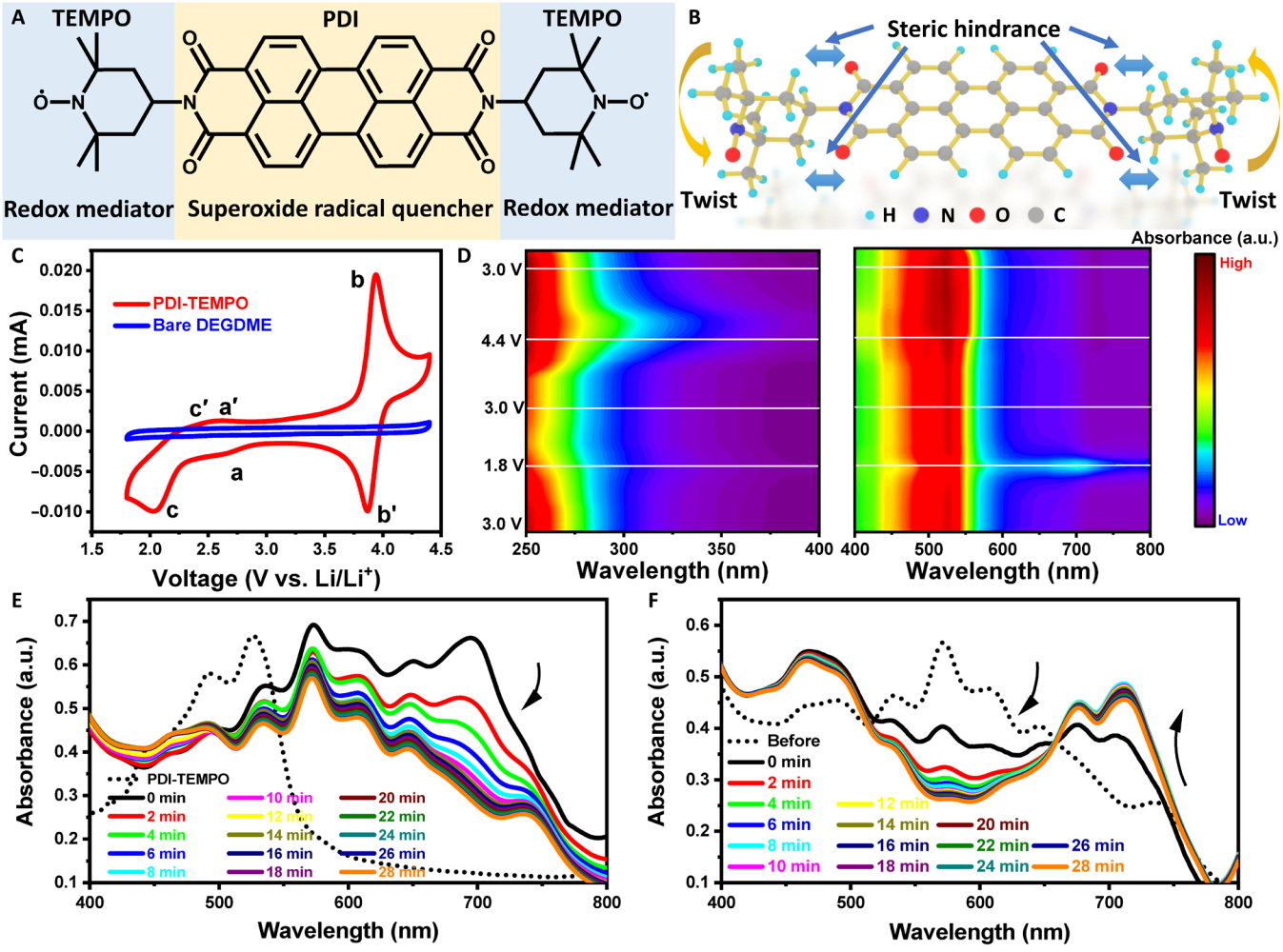

Fig. 1. Investigation of the redox capability of PDI-TEMPO in electrolytes. (**A**) The molecular structure and (**B**) stereostructure of PDI-TEMPO. a.u., arbitrary units. (**C**) CV curves of three-electrode cells with and without PDI-TEMPO in the DEGDME electrolyte in an argon atmosphere. The scan rate is 100 mV s^{-1}. The concentration of PDI-TEMPO is 5 mM. (**D**) In situ UV-Vis spectra of the electrolyte with PDI-TEMPO scanned in the range from 1.8 to 4.4 V. (**E** and **F**) UV-Vis spectra of the KO_2-saturated DMSO solution with PDI-TEMPO (E) before and (F) after the addition of lithium salt. The marked PDI-TEMPO spectrum in (E) is the original PDI-TEMPO/DMSO solution.

The electrochemistry of PDI-TEMPO has also been studied by in situ UV-Vis spectroscopy (Fig. 1D and fig. S6). During the potential scan from 3.0 to 1.8 V, the absorption band in the range of 250 to 350 nm associated with the TEMPO moieties gradually decreased, indicating that TEMPO moieties were reduced (fig. S6A). Simultaneously, the absorption band in the range of 450 to 550 nm associated with the pristine PDI backbone decreased, and the absorption at 700 nm from reduced PDI backbone increased (fig. S6B). The in situ UV-Vis spectroscopic study provides direct evidence that the PDI backbone has also been reduced following the reduction of the TEMPO moieties. Both reduction reactions are highly reversible because all absorption bands are recovered to their original states at the end of the reverse potential scan from 1.8 to 3.1 V (fig. S6, C and D). When the potential is further scanned to 3.6 V and beyond, the absorption band of the oxidized TEMPO moieties (250 to 350 nm) increases accordingly (fig. S6E) and recovers to their original intensities when the voltage is reversed to 3.0 V (fig. S6G). The peaks associated with the PDI backbone does not change because no redox reaction of PDI takes place in this potential range of 3.0 to 4.5 V (fig. S6, F and H). These results unambiguously confirm that there are three highly reversible redox reactions of PDI-TEMPO in the operation potential range of Li-O_2 batteries.

The redox behavior of PDI-TEMPO molecules has been further elucidated through density functional theory (DFT) calculations. Figure S7 shows the visualized lowest unoccupied molecular orbital (LUMO), highest occupied molecular orbital (HOMO), and singly occupied molecular orbital (SOMO) of PDI-TEMPO molecules. The HOMO is fully occupied with electrons and thereby can only provide electrons. Its energy level corresponds to the oxidation potential. Similarly, the LUMO can only accept electrons, and its energy level relates to the reduction potential. The SOMO, on the other hand, is partially occupied by one electron and therefore can both provide and accept electrons, and its energy level represents both oxidation and reduction potentials. Furthermore, the positions of the molecular orbitals also represent the possible sites where the redox reactions are most likely to occur. As shown in fig. S7A (left), both LUMO and HOMO are distributed on TEMPO moieties of PDI-TEMPO, suggesting that the initial oxidation and reduction reactions

of PDI-TEMPO are based on reversible redox reactions of TEMPO moieties. Similarly, as presented in fig. S7A (right), the SOMO of the oxidized PDI-TEMPO (PDI-TEMPO$^+$) is only distributed in TEMPO moieties, revealing that only TEMPO moieties are capable of being reduced (oxidized TEMPO moiety) and oxidized (neutral TEMPO moiety) at this stage. The SOMO of the reduced PDI-TEMPO (PDI-TEMPO$^-$) in fig. S7A (middle) mainly locates on the PDI core and one TEMPO moiety. This designates that the further reduction of PDI-TEMPO would occur on the PDI backbone, while the oxidation reaction would take place on the reduced TEMPO moiety. The DFT calculation results are consistent with the electrochemical studies (Fig. 1, C and D).

The oxidative and reductive capability of PDI-TEMPO molecules shown in fig. S7B reveals that the SOMO of the reduced PDI-TEMPO (−1) is higher than the LUMO of O_2. Therefore, the reduced PDI-TEMPO can reduce O_2 during the discharge process. The SOMO of the oxidized PDI-TEMPO (+1) is notably lower than the HOMO of Li_2O_2, suggesting that it can decompose Li_2O_2 during the charge process. Thus, PDI-TEMPO molecules can boost both discharge and charge processes of Li-O_2 batteries owing to their unique redox properties.

PDI-TEMPO molecule as a highly efficient $O_2^{\bullet-}$ quencher

PDI-TEMPO with the unique molecular and electronic structure can not only facilitate the formation and decomposition of Li_2O_2 via the redox-active TEMPO functional moieties but also effectively chemically eliminate $O_2^{\bullet-}$ through the conjugated PDI backbone as an $O_2^{\bullet-}$ quencher. Thus, the parasitic reactions originated from $O_2^{\bullet-}$ are expected to be substantially suppressed. We verified this hypothesis by dissolving potassium superoxide (KO_2) in the organic solvents, simulating the formation of $O_2^{\bullet-}$ during the discharge process. UV-Vis spectra were collected to monitor reactions between $O_2^{\bullet-}$ and PDI-TEMPO molecules (*51*). We used DMSO as the solvent because of the relatively high solubility of $O_2^{\bullet-}$ species in DMSO. After adding PDI-TEMPO into the KO_2-saturated DMSO, the UV-Vis absorption band corresponding to the original PDI-TEMPO (PDI^0-TEMPO, 450 to 550 nm) vanished immediately, and the band associated with the reduced PDI backbone (PDI$^-$-TEMPO, 700 nm) appeared initially but decreased with time (Fig. 1E). Meanwhile, a series of absorption peaks in the range of 500 to 650 nm emerged and remained. These newly formed peaks correspond to the reduced PDI backbone with the acceptance of two electrons (PDI^{2-}-TEMPO) (*42*). This reduction process is accompanied by a color change of the solution from red to brown and, lastly, blue (fig. S8). Therefore, the PDI backbone can be easily reduced by $O_2^{\bullet-}$ (fig. S9A). After adding lithium salt [lithium bis(trifluoromethanesulfonyl)imide (LiTFSI)] in the aforementioned reduced PDI-TEMPO solution, the UV absorption associated with the PDI^{2-}-TEMPO species gradually vanished, while the peaks corresponding to PDI^0-TEMPO and PDI$^-$-TEMPO reappeared (Fig. 1F). This phenomenon indicates that the reduced PDI backbone can be easily oxidized by $O_2^{\bullet-}$ when lithium salt is present (fig. S9B). As there are still $O_2^{\bullet-}$ presenting in the electrolyte, the PDI-TEMPO can still be reduced by $O_2^{\bullet-}$ and then oxidized by lithium salt and $O_2^{\bullet-}$ (fig. S9B). This is a dynamic process that lithium salt and superoxide radicals are continuously consumed to form Li_2O_2, facilitated by the chemical quenching reactions with PDI-TEMPO. This mechanism was further confirmed by EPR studies. The EPR peaks generated from the combination of 5,5-dimethyl-1-pyrroline *N*-oxide (DMPO) and $O_2^{\bullet-}$ gradually disappeared after adding PDI-TEMPO and lithium salt (fig. S10). The chemical reactions between PDI-TEMPO and $O_2^{\bullet-}$ are proposed as below

$$PDI^0 - TEMPO + O_2^- \rightarrow PDI^- - TEMPO + O_2 \quad (1)$$

$$PDI^- - TEMPO + O_2^- \rightarrow PDI^{2-} - TEMPO + O_2 \quad (2)$$

$$PDI^{2-} - TEMPO + O_2^- + 2Li^+ \rightarrow PDI^- - TEMPO + Li_2O_2 \quad (3)$$

$$PDI^- - TEMPO + O_2^- + 2Li^+ \rightarrow PDI^0 - TEMPO + Li_2O_2 \quad (4)$$

Overall reaction

$$2O_2^- + 2Li^+ \rightarrow Li_2O_2 + O_2 \quad (5)$$

On the basis of the above experimental results, PDI-TEMPO molecules are confirmed to be a reusable soluble $O_2^{\bullet-}$ quencher, which efficiently eliminates $O_2^{\bullet-}$ by chemically reacting with $O_2^{\bullet-}$ to form Li_2O_2. As a result, the $O_2^{\bullet-}$ species will be immediately consumed once they are generated, and the parasitic reactions induced by $O_2^{\bullet-}$ will be dramatically diminished. Furthermore, the multistep chemical reactions between $O_2^{\bullet-}$ and PDI-TEMPO detour around the self-disproportion reactions of $O_2^{\bullet-}$ (LiO_2), which significantly suppresses the generation of $^1O_2$, eliminating parasitic reactions associated with $^1O_2$ as well (fig. S4) (*41*, *45*, *46*). The deactivation of $O_2^{\bullet-}$ by PDI-TEMPO has been further demonstrated by monitoring the reaction of KO_2 and DEGDME electrolyte for 1 week (fig. S11). The FTIR spectra of the DEGDME electrolyte containing PDI-TEMPO show no obvious change after a 1-week reaction, suggesting no detectable parasitic reactions between $O_2^{\bullet-}$ and DEGDME solvent. However, the FTIR spectrum of the control sample (no PDI-TEMPO) shows an increase in peak at 1650 cm^{-1}, which signifies the formation of C═O, because of the attack by active oxygen species. Therefore, PDI-TEMPO in the electrolyte can simultaneously diminish parasitic reactions and promote the formation of Li_2O_2.

Discharge behavior of Li-O_2 batteries with PDI-TEMPO molecules

The electrochemistry of PDI-TEMPO was examined with CV using a GC electrode in an electrolytic cell. As shown in fig. S12, the ORR peak current in the PDI-TEMPO electrolyte is much higher than that in the bare DEGDME electrolyte. This clearly corroborates the PDI-TEMPO's capability of facilitating the discharge process. Similar results have also been obtained with an Li-O_2 cell containing a carbon paper positive electrode and a lithium foil negative electrode (figs. S13 and S14). Figure 2A shows the discharge-charge profiles of an Li-O_2 cell with a cutoff voltage of 2.0 and 4.6 V. The cell with PDI-TEMPO electrolyte delivers a specific capacity of 4.5 mAh cm^{-2}, which is more than 46 times higher than that of the cell with bare DEGDME electrolyte (less than 0.1 mAh cm^{-2}; Fig. 2A and fig. S15). It is worth noting that the same configurated cell with PDI-TEMPO electrolyte operated in an argon atmosphere only provides a specific capacity of 0.02 mAh cm^{-2} (fig. S16), which is negligible compared with the capacity obtained in the oxygen atmosphere. Therefore, the high specific capacity should be entirely ascribed to the reversible formation and decomposition of Li_2O_2 (figs. S17 to S18), instead of the redox reaction of PDI-TEMPO dissolved in the electrolyte.

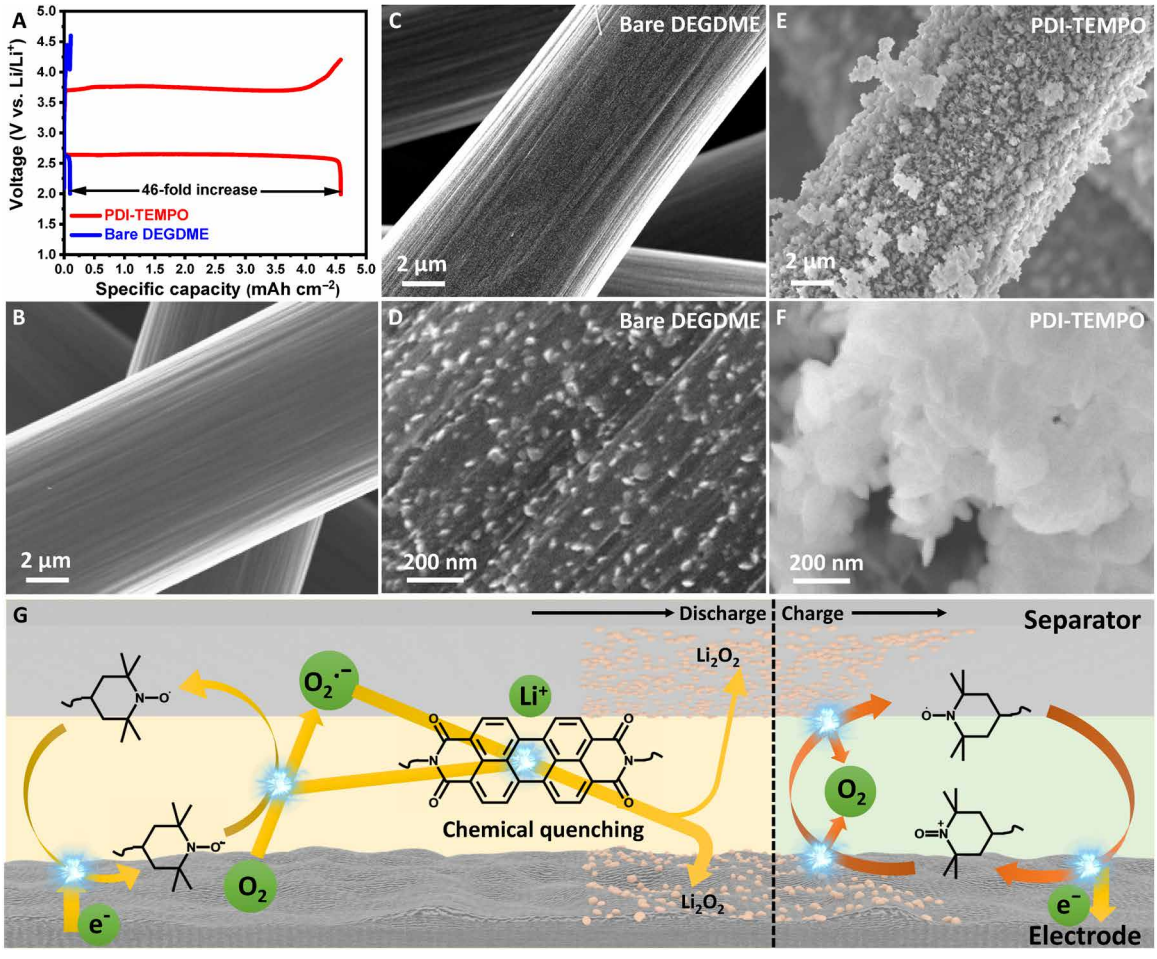

Fig. 2. Improvement of Li-O_2 batteries with the aid of PDI-TEMPO. (**A**) Full discharge-charge profiles of Li-O_2 batteries with PDI-TEMPO electrolyte and bare DEGDME electrolyte. Lithium foils are used as the anodes, and carbon papers as the cathodes. The current density is 0.1 mA cm^{-2}. The concentration of PDI-TEMPO is 5 mM. SEM images of the carbon paper electrodes (**B**) before and (**C** to **F**) after the first discharge. The electrolytes used are (C and D) bare DEGDME electrolyte and (E and F) PDI-TEMPO electrolyte. (**G**) Schematic illustration of the PDI-TEMPO facilitating the formation and decomposition of Li_2O_2 during the operation of Li-O_2 batteries.

The morphologies of discharged Li_2O_2 on the carbon paper electrode after the first discharge were characterized by scanning electron microscopy (SEM). Comparing to the pristine morphology in Fig. 2B, only a small amount of discharge products are observed on carbon fibers when discharged in the bare DEGDME electrolyte (Fig. 2, C and D). On the contrary, a large quantity of Li_2O_2 was generated on carbon fibers in the PDI-TEMPO electrolyte (Fig. 2, E and F). The cells with PDI-TEMPO electrolyte produced Li_2O_2 nanoparticles as the discharge product, which is different from the toroidal-shaped Li_2O_2 commonly obtained through a solution mechanism (fig. S19) (*52*, *53*). This indicates that the discharge process may proceed via a different mechanism. We propose a chemical quenching process of $O_2^{\bullet-}$ by PDI-TEMPO molecules (*54*). As schematically shown in Fig. 2G, the discharge of the Li-O_2 cell is initiated by the reduction of TEMPO moieties, which reacts with oxygen molecules to catalyze the ORR process. The reduced oxygen species are then either directly released into the electrolyte or interacted with the reduced TEMPO moieties, which are then chemically quenched by the PDI backbone to generate Li_2O_2 nanoparticles. Therefore, the entire discharge process is mainly driven by the chemical quenching of $O_2^{\bullet-}$ in the electrolyte, which has also been verified by the rotating ring-disk electrode (RRDE) measurements (figs. S20 and S21) (*55*). The above process is further enhanced when carbon nanotube (CNT) electrodes with higher specific surface area are used to accelerate the formation of $O_2^{\bullet-}$ (figs. S22 to S25). The results clearly corroborate that PDI-TEMPO molecules can efficiently relay electrons from the electrode surface to the dissolved O_2 to produce $O_2^{\bullet-}$. Meanwhile, the $O_2^{\bullet-}$ can be chemically disproportionated to Li_2O_2 with the assistance of PDI backbones simultaneously (figs. S26 and S27 and movie S1).

Charge behavior of Li-O_2 batteries with PDI-TEMPO molecules

The PDI-TEMPO molecules can also function as a charging reaction redox mediator to efficiently improve the round-trip efficiency for Li-O_2 batteries (fig. S28). As shown in Fig. 2A and figs. S29 and S30, the charge voltage has been significantly decreased to 3.7 V (compared with 4.2 V in bare DEGDME electrolyte). This result is consistent with the CV curves (Fig. 1C), indicating that the redox reaction of PDI-TEMPO is responsible for the decrease in the charge overpotentials of the Li-O_2 cells.

To further analyze the discharge-charge process, galvanostatic intermittent titration technique (GITT) was conducted during the

discharge and charge processes. As shown in Fig. 3A, the discharge curves and the open-circuit potentials in the PDI-TEMPO electrolyte are more stable than that in the bare DEGDME electrolyte, owing to fast discharge kinetics in the PDI-TEMPO electrolyte. During charging, the equilibrium potentials of the cell with PDI-TEMPO electrolyte are much lower, ascribed to fast kinetics of Li_2O_2 decomposition in PDI-TEMPO electrolyte (Fig. 3B and fig. S31). Moreover, the enlarged GITT curves in the bare DEGDME electrolyte show three distinguishable charge stages (*10*, *56*). The first stage (0 to 0.15 mAh cm^{-2}) displays a linear increase in voltage during the charge scan, which could be ascribed to the delithiation of the Li_2O_2 in the initial charge process. The second stage (0.15 to 0.35 mAh cm^{-2}) presents a temporary increase but followed by a drop of the charge voltage during each charge scan, indicating a typical Li_2O_2 decomposition through the nucleation process. The third stage (0.35 to 0.5 mAh cm^{-2}) exhibits a flat increase in the voltage, which may originate from the mixed reactions of Li_2O_2 decomposition and parasitic reactions at high overpotential. The GITT curves in PDI-TEMPO, however, show no divided charge stages. A flat plateau is observed, without temporary increase in charge voltage at each charge step, owing to the lack of typical Li_2O_2 decomposition through the nucleation process. Therefore, the charge process in the Li-O_2 cell with PDI-TEMPO electrolyte proceeds through a different mechanism from those in the cell with bare DEGDME electrolyte. The charge process is triggered and accelerated by the chemical reaction between oxidized TEMPO moieties in PDI-TEMPO molecules and solid Li_2O_2, as well as the quenching reaction between PDI-TEMPO and released superoxide species. Therefore, it proves that PDI-TEMPO can efficiently accelerate the kinetics of the OER.

The charging reaction has been further studied by a quantitative in situ differential electrochemical mass spectrometry (DEMS) using less volatile tetraethylene glycol dimethyl ether (TEGDME) electrolyte, during which the O_2 evolved and the charge passed were monitored simultaneously. The oxygen evolution during the charge process with ether electrolyte has the same trend as the GITT results. A peak increase in the evolution at the initial stage is followed by a sharp decrease before the evolution increases again in the middle of the charge process (Fig. 3C). This corresponds to a typical Li_2O_2 decomposition through a nucleation process (*10*, *41*, *56*). The oxygen evolution in the PDI-TEMPO electrolyte shows a steady curve from the initial stage of charge. It proves that the chemical reaction between the oxidized PDI-TEMPO and Li_2O_2 dominates the charge process (Fig. 3D). The ratio of the charge passed and the O_2 evolved during charging of the Li-O_2 battery has been quantified to be 2.01 e^-/O_2, while for bare Li-O_2 cell, a 2.40 e^-/O_2 has been obtained. The enhanced charging reversibility confirms that PDI-TEMPO can also efficiently promote the charge process.

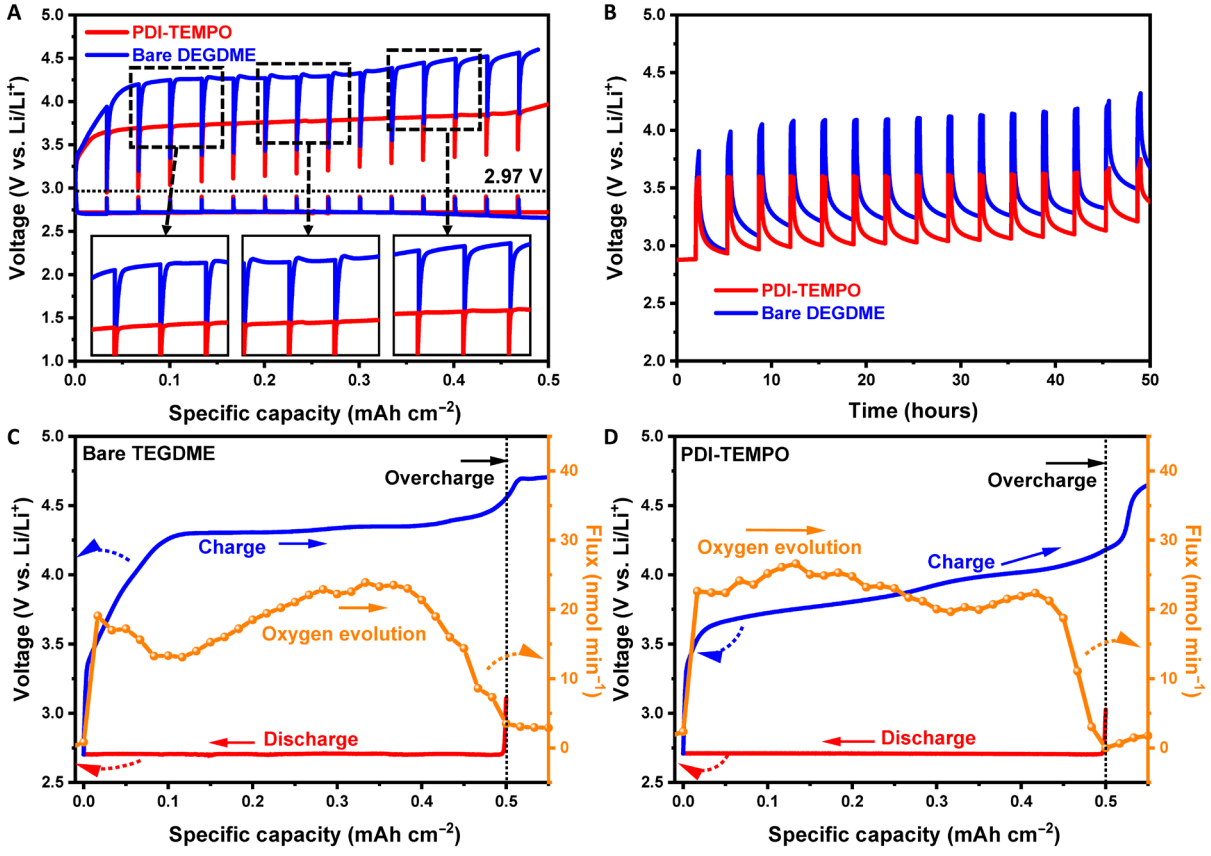

Fig. 3. Investigation of mechanisms within Li-O_2 batteries using PDI-TEMPO electrolyte. (**A** and **B**) GITT curves of the Li-O_2 batteries, which were acquired with a current density of 0.1 mA cm^{-2} for 0.5 mAh cm^{-2} and (A) a 60-min or (B) a 180-min time interval during the discharge and (B) charge processes. The insets are the enlarged images of selected areas. The concentration of PDI-TEMPO is 5 mM. (**C** and **D**) In situ DEMS analysis of the gas evolution during the charge process of Li-O_2 cell operation with (C) bare TEGDME electrolyte and (D) PDI-TEMPO electrolyte. The current density is 0.1 mA cm^{-2}.

PDI-TEMPO molecules to suppress parasitic reactions

The cycling performance of Li-O_2 cells containing PDI-TEMPO molecules has been markedly improved (Fig. 4, A and B, and figs. S32 and S33), because PDI-TEMPO molecules act as an $O_2^{\bullet-}$ quencher to eliminate active $O_2^{\bullet-}$ species and expedite both discharge and charge processes. Compared with only 39 cycles delivered by the Li-O_2 cell with bare DEGDME electrolyte, the cell with PDI-TEMPO electrolyte has shown a stable cycling performance over 300 cycles (Fig. 4B). As shown in Fig. 4A, the cell with PDI-TEMPO electrolyte displays stable charge potentials around 3.7 V during cycling, which is about 0.7 V lower than the cell with bare DEGDME electrolyte. The excellent electrochemical performance should be ascribed to the unique functions of PDI-TEMPO, which can efficiently diminish parasitic reactions and promote discharge and charge processes. To prove this point, we performed postmortem FTIR and x-ray diffraction (XRD) characterizations on the cathodes after cycling (Fig. 4, C to F). The discharge products were dominated by Li_2O_2 after the first discharge with PDI-TEMPO electrolyte, because strong FTIR peaks were found in the range of 400 to 700 cm^{-1}, and no peaks were spotted in the range of 1300 to 1700 cm^{-1} in either electrolyte. These FTIR peaks disappeared after the first charge process, indicating highly reversible formation and decomposition of Li_2O_2 during discharge and charge processes. However, the FTIR peaks at 400 to 700 cm^{-1} in bare DEGDME electrolyte remained in the charge process after five cycles, and the peaks associated with Li_2CO_3 in the range of 1300 to 1700 cm^{-1} increased gradually with cycling (Fig. 4C). This confirms that a large quantity of Li_2CO_3 accumulated after several cycles in the bare DEGDME electrolyte. On the contrary, the FTIR peaks in the range of 400 to 700 cm^{-1} reversibly appeared and disappeared after discharge and charge processes in PDI-TEMPO electrolyte, corroborating that Li_2O_2 is the dominant discharge product (Fig. 4D). The XRD patterns of the corresponding cathodes also confirm the same conclusion. The XRD peaks of Li_2O_2 became weaker on cycling and eventually disappeared after 10 cycles when using bare DEGDME electrolyte (Fig. 4E). The XRD peaks of Li_2O_2 remained visible after 25 cycles in PDI-TEMPO electrolyte (Fig. 4F).

The accumulation of by-products in the bare DEGDME electrolyte originates from parasitic reactions of active oxygen species ($O_2^{\bullet-}$ and $^1O_2$) and the decomposition of electrolyte solvent. The continuous attack by $O_2^{\bullet-}$ and $^1O_2$ to solvent molecules and cathode materials lead to the formation of a substantial amount of by-products during cycling. Moreover, high charging voltage is required to decompose both Li_2O_2 and by-products, resulting in the further decomposition of electrolyte solvent and generation of more $^1O_2$. This vicious cycle continuously produces by-products and eventually terminates the Li-O_2 batteries. It is worth noting that adding TEMPO, a commonly used redox mediator, in the DEGDME electrolyte to lower the charge potential can also suppress parasitic reactions associated with large overpotentials to a certain extent during the charge process (fig. S34). It has recently been reported by Petit *et al.* and Liang *et al.* that the use of redox mediators could accelerate the relaxation of $^1O_2$, making them a potential quencher for $^1O_2$ (*41*, *57*). However, we found that the cell with TEMPO redox mediator could only last for 60 cycles, and by-products still quickly accumulated during cycling (fig. S34).

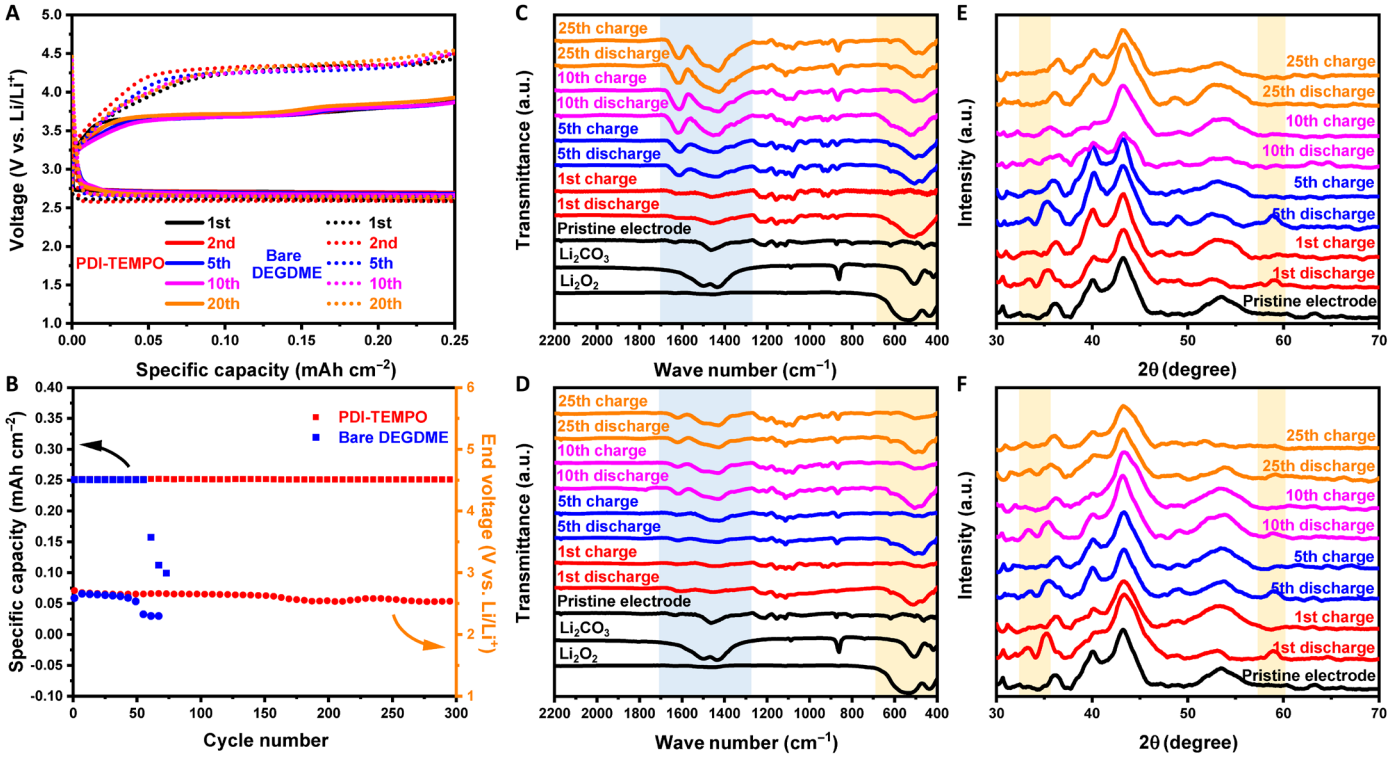

Fig. 4. Postmortem characterizations of electrodes after cycling. (**A**) The discharge-charge profiles and (**B**) cycling performance of Li-O_2 batteries with PDI-TEMPO electrolyte and DEGDME electrolyte. The reversible capacities are restricted to 0.25 mAh cm^{-2}. The current densities are 0.1 mA cm^{-2}, and the cutoff voltage is 2.3 V/4.6 V. The concentration of PDI-TEMPO is 5 mM. (**C** and **D**) Postmortem FTIR spectra of electrodes after cycling with (C) bare DEGDME electrolyte and (D) PDI-TEMPO electrolyte. (**E** and **F**) Postmortem XRD patterns of the electrodes after cycles with (E) bare DEGDME electrolyte and (F) PDI-TEMPO electrolyte. The highlighted blue areas are the places where the characteristic peaks for Li_2CO_3 appear, and the highlighted orange areas are the places where the characteristic peaks for Li_2O_2 appear.

This specifies that parasitic reactions associated with active oxygen species attack during the discharge and charge processes remained severe. The rational design of PDI-TEMPO molecules can efficiently lower the charge overpotentials and quench $O_2^{\bullet-}$ species, both of which are deemed as the origins of $^1O_2$ generation. Furthermore, TEMPO moieties are also reported to accelerate the relaxation of $^1O_2$ during the operation of Li-O_2 batteries, and two TEMPO moieties bridged by PDI backbone in one molecule probably enhance their overall capability in quenching $^1O_2$ (*41*, *57*). Therefore, PDI-TEMPO molecules are able to suppress the generation of $^1O_2$ as well, leading to the comprehensive suppression of parasitic reactions. To verify this assertion, we conducted a demonstration experiment by adding 20 mM 9,10-dimethylanthracene (DMA) in electrolytes as the trap agent for $^1O_2$. The results in fig. S35 show that DMA is quickly consumed in DEGDME electrolyte over cycling, while TEMPO electrolyte displays a much lower consumption rate of DMA. The consumption rate of DMA in PDI-TEMPO electrolyte is the slowest, which almost equals the self-degradation rate of DMA in O_2 atmosphere. This result unambiguously verifies that PDI-TEMPO molecules can not only quench superoxide radicals and lower charge overpotentials but also suppress the generation of $^1O_2$, leading to substantially reduced parasitic reactions.

Cycling performance of Li-O_2 batteries with PDI-TEMPO molecules

Unlike previously reported redox mediators that can easily shuttle to the negative electrode and react with the highly active lithium metal, PDI-TEMPO molecules can effectively overcome this issue in Li-O_2 batteries. Our rationally designed PDI-TEMPO molecules contain a conjugated PDI backbone and two bulky TEMPO moieties. The steric hindrance between these two segments results in a twisted stereostructure of PDI-TEMPO molecule, in which TEMPO moieties are not on the same plane as the PDI backbone (Fig. 1B and fig. S36, A and B). This distinctive stereostructure enables PDI-TEMPO molecules to be restricted in the cathode region by van Der Waals forces via π-π interactions between the conjugated PDI backbone and the conjugated graphitic carbon in the cathodes (fig. S36C) (*42*, *47*, *50*). Meanwhile, such π-π interactions are weakened by the steric hindrance between the graphitic carbon and bulky TEMPO moieties, preventing PDI-TEMPO molecules from depositing on the cathode (Fig. 5A and fig. S36C). Consequently, PDI-TEMPO molecules are still in the electrolyte, but prohibited from migrating to lithium anode and reacting with lithium metal. Moreover, because PDI-TEMPO molecules quench the reduced oxygen species immediately after they are generated, these species are also restricted to the cathode region to form discharge products (fig. S26). Therefore, PDI-TEMPO molecules can also strongly inhibit parasitic reactions on lithium metal anodes from these small molecules. To verify this, lithium metal anodes were characterized by SEM after cycling. A comparison experiment was conducted by dissolving 10 mM TEMPO in DEGDME electrolyte. As shown in fig. S37, the lithium foil retrieved from TEMPO electrolyte is severely corroded, caused by the direct reactions between lithium metal and oxidized TEMPO molecules. The lithium foil in the bare DEGDME electrolyte also shows a corroded morphology (Fig. 5B), which originates from the parasitic reactions between lithium metal and the dissolved small molecules such as oxygen species (fig. S38). On the contrast, the lithium foil in PDI-TEMPO electrolyte shows no obvious corrosion after cycling

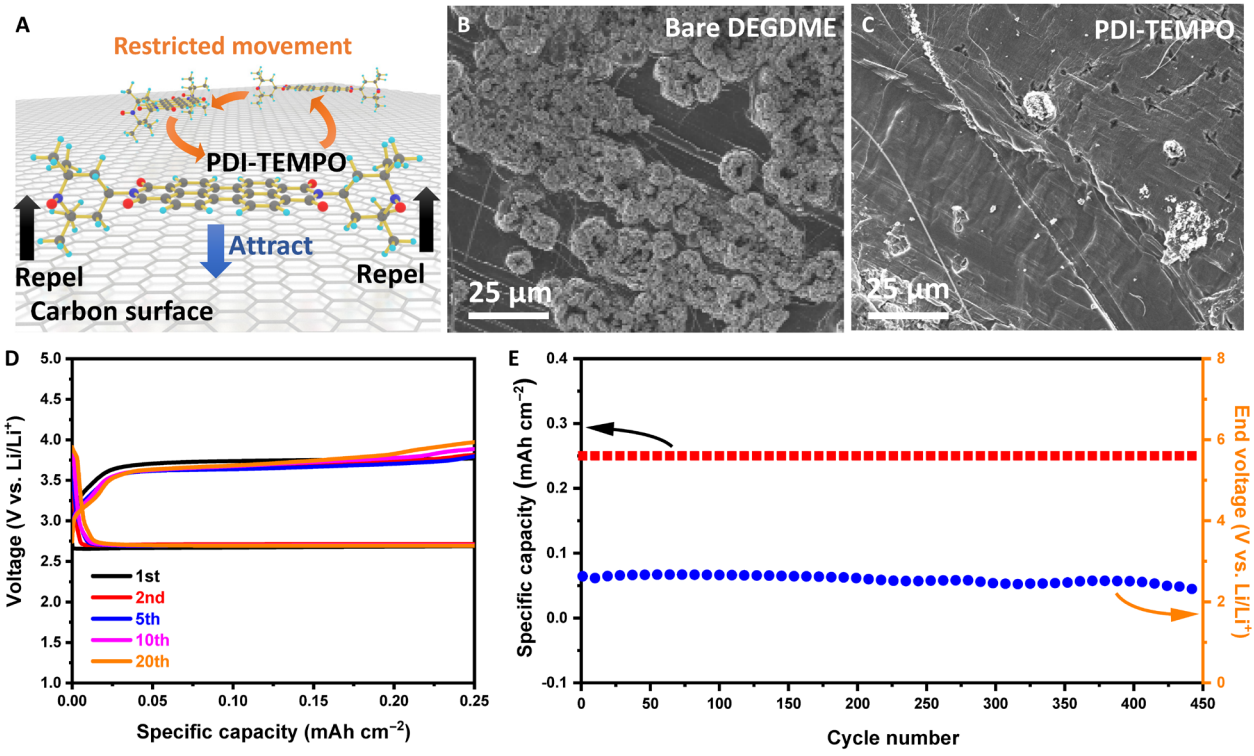

Fig. 5. Influences of PDI-TEMPO on lithium metal anode and cycling performance. (**A**) Schematic illustration of the interaction between PDI-TEMPO and graphitic carbon. (**B** and **C**) SEM images of the lithium metal anodes from (B) bare DEGDME electrolyte and (C) PDI-TEMPO electrolyte after 10 cycles. (**D**) Discharge-charge profiles and (**E**) cycling performance of the Li-O_2 batteries with 10 mM PDI-TEMPO electrolyte. The current density is 0.2 mA cm^{-2}.

(Fig. 5C), demonstrating that PDI-TEMPO molecules can suppress parasitic reactions caused by the dissolved oxygen species. Therefore, further increasing the concentration of PDI-TEMPO in the electrolyte until 10 mM should not deteriorate the electrochemical performance (concentration optimization in fig. S39). Instead, high concentration of PDI-TEMPO enhances its capability for quenching $O_2^{\bullet-}$ and suppressing $^1O_2$, especially at elevated current densities (fig. S40). Hence, we subsequently doubled the concentration of PDI-TEMPO to 10 mM in electrolyte. As shown in Fig. 5D, the Li-O_2 cell with 10 mM PDI-TEMPO electrolyte presents low overpotentials and a significantly extended cycle life of more than 450 cycles (Fig. 5E and fig. S41). We further incorporated a Nafion membrane on lithium metal to prevent the dendrite growth and a porous graphene electrode to accommodate more Li_2O_2 (figs. S42 to S44). The Li-O_2 cell with PDI-TEMPO reagent has exhibited an ultralong cycle life exceeding 1400 cycles (fig. S45) (*58*).

DISCUSSION

In summary, a multifunctional PDI-TEMPO quencher has been rationally designed and synthesized for boosting the performance of Li-O_2 batteries. The PDI-TEMPO molecule contains a PDI backbone with the capability of quenching $O_2^{\bullet-}$, and redox mediator-active TEMPO moieties to catalyze both discharge and charge processes in the electrolyte solution. When added in the DEGDME electrolyte, the operation of the Li-O_2 cell undergoes a new chemical-quenching reaction mechanism, leading to the formation of Li_2O_2 nanoparticles. Furthermore, the unique twisted molecular structure confines PDI-TEMPO molecules in the cathode region, which can effectively prevent corrosion of lithium metal anode. Consequently, Li-O_2 cells containing PDI-TEMPO quencher demonstrated an increased discharge capacity, improved energy efficiency, diminished parasitic reactions, and long cycle life.

MATERIALS AND METHODS

Synthesis of PDI-TEMPO

The detailed synthesis process of *N*,*N*′-di-(2,2,6,6-tetramethyl-1-oxyl-4-piperidinyl)-perylene-3,4,9,10-tetracarboxylic diimide (PDI-TEMPO) is illustrated in fig. S1A (*42*, *43*).

In brief, 0.51 ml (3 mmol) of 4-amino-2,2,6,6-tetramethylpiperidine (Sigma-Aldrich), 0.588 g (1.5 mmol) of perylene-3,4,9,10-tetracarboxylic dianhydride (Sigma-Aldrich), and 0.279 g (1.5 mmol) of zinc acetate (Sigma-Aldrich) were combined with 25 g of imidazole (Sigma-Aldrich) in a round bottle flask. The flask was evacuated and refilled with argon three times and then heated with a sand bath at 120°C for 3 hours, 160°C for 3 hours, 200°C for 3 hours, and, lastly, 240°C for 48 hours. After the mixture cools down to ~80°C, 200 ml of $CHCl_3$ was carefully added to the flask. The clear red solution was extracted by separatory funnel and washed five times with 50 ml of water. The obtained organic phase was then collected, dried over $MgSO_4$, and concentrated under reduced pressure to yield a purple solid (PDI-TEMPH).

The resulting compound PDI-TEMPH was further oxidized by dissolving in methanol at room temperature together with a catalytic amount of $Na_2WO_4{\cdot}2H_2O$ (Sigma-Aldrich) and 5 ml of 30% H_2O_2 (ChemSupply) (*37*, *48*). The mixture was stirred at room temperature for 24 hours. After the reaction, the solvents were removed through Rotavapor (Buchi R-100), and isopropanol (Sigma-Aldrich) was added to dissolve the crude product. After filtration, the filtrate was collected and dried under vacuum at room temperature. PDI-TEMPO was obtained as a purple-reddish solid. The solid was dried under vacuum for 24 hours before storing in the argon-filled glovebox. PDI-TEMPO can also be prepared by the direct reaction between 4-amino-2,2,6,6-tetramethylpiperidine-1-oxyl and perylene-3,4,9,10-tetracarboxylic dianhydride via a similar process, without the oxidation process.

Characterizations

The ^{1}H nuclear magnetic resonance spectra were recorded on an Agilent 500 Spectrometer at 25°C in d-chloroform. The infrared spectroscopy measurements were conducted on a Nicolet Magna 6700 FT-IR spectrometer. All spectra were obtained using 4-cm^{-1} resolution and 64 scans at room temperature. The spectra of ATR-FTIR were obtained using 4-cm^{-1} resolution and 16 scans at room temperature with argon protection. A field emission scanning electron microscope (Zeiss Supra 55 VP) was used to observe the electrode morphologies. Nitrogen-sorption measurements were carried out at 77 K with a Micromeritics 3Flex surface characterization analyzer. The specific surface area was calculated by the Brunauer-Emmett-Teller (BET) method. UV-Vis spectroscopy was conducted through an Agilent Cary 60 UV-Vis spectrophotometer, scanning from 800 to 200 nm. All the electrospray ionization–MS spectra were recorded on Waters liquid chromatography–MS system with the condition setting as follows: capillary voltage, 3.0 kV; extractor voltage, 2.0 V; RF lens, 0.5 V; source temperature, 120°C; desolvation temperature, 200°C; desolvation gas flow, 500 liter $hour^{-1}$; pump flow, 20 μl min^{-1}. Sample concentration was 1 to 5 mg μl^{-1} in MeOH, and the cone voltage was varied from 15 to 80 V depending on the samples. EPR was collected using a Bruker EMX X-Band ESR Spectrometer. EPR spectra were obtained under 120 K and then normalized on the basis of the weight of the samples used for measurement. XRD measurement was performed on a Bruker D8 X-ray diffractometer using Cu Kα radiation. For the XRD analysis, the electrodes from the disassembled cells were washed and dried first and then sealed with "Parafilm" to exclude moisture and carbon dioxide from the discharge products, which are very sensitive to normal atmospheric air components.

Electrochemical characterizations

All the electrochemical characterizations were conducted on a CH Instruments 660E electrochemical workstation and BioLogic VMP3 potentiostat. The CV for two-electrode configuration was operated by using a lithium metal foil as the anode, glass fibers as separator soaking with electrolyte, and a porous electrode as the cathode. Carbon paper electrodes were prepared by stacking three layers of precut carbon papers (10-mm diameter). CNT cathodes were prepared by casting the slurry of CNT and polytetrafluoroethylene (PTFE) (8:2) in iso-propylene/water on the precut carbon paper and dried before use. Porous graphene electrodes were prepared via the same method (*59*). The electrolyte was prepared by dissolving 5 mM PDI-TEMPO in DEGDME with 0.5 M LiTFSI. The scan rate was 0.5 mV s^{-1}. The CV for three-electrode configuration was operated with a Pt wire as the counter electrode, an Ag wire as the reference electrode, and a GC electrode as the working electrode. The scan rate was 100 mV s^{-1}.

The discharge/charge performances were evaluated by a Neware Battery Testing System. The discharge-charge performances were

evaluated by assembling Li-O_2 batteries. A two-electrode Swagelok-type cell with an air hole (0.785 cm^2) on the cathode side was used to test the electrochemical performances. A two-electrode coin cell (CR2033, Neware) with several open holes on the cathode side was used for long-term cycling. The cells were assembled in an argon-filled glove box with water and oxygen level less than 0.1 parts per million. Lithium foils were used as anodes, and polyvinylidene difluoride (PVDF)/glass fibers were used as separators. The lithium foils were immersed in propylene carbonate solution containing 5% fluoroethylene carbonate for 5 days before use. A Nafion membrane was used between the lithium anode and separator for long-term cycling. The electrolytes were prepared by dissolving 0.5 M LiTFSI in DEGDME with 5 mM PDI-TEMPO. The typical amount of electrolyte used in a single cell was 150 μl. The assembled cell was gas-tight except for the cathode side window, which is exposed to the oxygen tank. All measurements of Li-O_2 batteries were conducted in a gas tank of 1-atm dry oxygen atmosphere. The capacities of the batteries were calculated on the basis of the total area of the electrodes. GITT was performed using an Li-O_2 cell at a current density of 0.1 mA cm^{-2}. A 1-hour/3-hour rest step was given after 10 min of each discharge and charge step. The cutoff capacity was set to 0.5 mAh cm^{-2}.

A modified Swagelok-type Li-O_2 cell was linked to a commercial magnetic sector mass spectrometer (Thermo Fisher Scientific) by a specially designed gas-purging system for in situ DEMS measurement. The flow rate of purge gas was set at 1 ml min^{-1}. During the charge process, high-purity Ar was used as the carrier gas. The DEMS cells were assembled in the argon-filled glove box for the electrochemical testing.

The RRDE measurements were performed using an RRDE with a GC disk and a Pt ring (Pine Research Instrumentation, USA) (*55*). A homemade three-electrode configuration was used with Pt wire as the counter electrode, Ag wire as the reference electrode, and RRDE as the working electrode. The electrolytes used for the measurements were the DEGDME electrolyte and PDI-TEMPO electrolyte. To prevent potential mask effect by the redox current of PDI-TEMPO, the PDI-TEMPO electrolyte was prepared by dissolving 0.5 mM PDI-TEMPO in the DEGDME electrolyte. The rotation speed of the RRDE was held at 1600 rpm for the tests. To ensure the generation of currents for OER and ORR from both electrolytes during the tests, an oxidation potential was held constantly at 4.1 V versus Li/Li^+, and a reduction potential was held constantly at 2.3 V versus Li/Li^+. As the currents generated for OER come from the consumption of Li_2O_2, which was generated during the ORR process, the tests of the OER efficiency were conducted straight after tests of the ORR efficiency. The tests of the ORR efficiency were carried out in the oxygen atmosphere, and the ones of the OER efficiency were in the argon atmosphere. To further eliminate the currents from side reactions and self-redox reactions, a control experiment was carried out using the same setting and only operated all the measurements in the argon atmosphere. The calculation of the efficiency could be corrected by the equation below

$$\text{Efficiency} = (I_{\text{ring}} - I_{\text{ring–correction}})/(I_{\text{disk}} - I_{\text{disk–correction}}) \quad (6)$$

The I_{ring} and I_{disk} are the currents obtained on the ring and disk electrodes during the ORR and OER processes. The $I_{\text{ring-correction}}$ and $I_{\text{disk-correction}}$ are the currents obtained on the ring and disk electrodes during the control experiment. More details will be found in the illustration in figs. S20 and S21.

Theoretical calculations

The HOMO and LUMO in this work were performed with the Gaussian 09 program, through the conventional DFT calculations using the hybrid exchange-correlation functional B3LYP on the molecules. The Basis Set was triple-zeta valence with polarization (TZVP) (*60*).

Demonstration experiments

The demonstration experiments of the scattering of Li_2O_2 during the discharge process were performed by assembling the Li-O_2 cell through a special configuration. A carbon paper was added between the lithium anode and the glass fiber separator. CNT electrodes were used as cathodes in the cell. The cell was directly discharged to 2.0 V at a current density of 0.1 mA cm^{-2}. The inserted carbon paper was taken out for SEM, and the glass fiber was taken out for phenolphthalein tests. The phenolphthalein tests were performed by first soaking the glass fiber into 3 ml of water. Then, two drops of freshly made phenolphthalein/ethanol solution were added to the aqueous solution dropwise. The color-changing process was recorded by video and photoshoots.

The demonstration of the capacity loss during the charge process was performed by changing the electrolyte/separator after the discharge process. The Li-O_2 cells with different electrolyte configuration were first discharged to 0.25 mAh cm^{-2} at a current density of 0.1 mA cm^{-2}. The cells were then taken to an argon-filled glove box and dissembled. The cathodes were washed with clean DEGDME solvent three times and dried under vacuum. The dried cathodes were then assembled into Li-O_2 cells with fresh lithium metal anodes, a glass fiber separator soaked with DEGDME electrolyte. The as-assembled cells were then directly charged to 4.6 V at a current density of 0.1 mA cm^{-2}.

The demonstration of the suppression of $^1O_2$ during cycling was performed by adding 20 mM DMA in all the electrolytes. To avoid possible reactions between lithium metal and DMA, an $LiFePO_4$/C electrode was used instead of the lithium metal foil as the anode. The Li-O_2 cells were cycled with a capacity of 0.25 mAh cm^{-2} at a current density of 0.1 mA cm^{-2}. The cells were then taken to an argon-filled glove box and dissembled. All the battery components were soaked in 9 ml of DEGDME solvent. UV spectra were performed on the extracted solution. A reference was prepared by resting the bare DEGDME electrolyte with 20 mM DMA in oxygen for the same time of each cycling period to monitor the self-degradation of DMA in O_2.

SUPPLEMENTARY MATERIALS

Supplementary material for this article is available at https://science.org/doi/10.1126/sciadv.abm1899

REFERENCES AND NOTES

1. C. Xia, C. Kwok, L. Nazar, A high-energy-density lithium-oxygen battery based on a reversible four-electron conversion to lithium oxide. *Science* **361**, 777–781 (2018).
2. J. Lu, L. Li, J.-B. Park, Y.-K. Sun, F. Wu, K. Amine, Aprotic and aqueous Li–O_2 batteries. *Chem. Rev.* **114**, 5611–5640 (2014).
3. A. C. Luntz, B. D. McCloskey, Nonaqueous Li-air batteries: A status report. *Chem. Rev.* **114**, 11721–11750 (2014).
4. T. Liu, J. P. Vivek, E. W. Zhao, J. Lei, N. Garcia-Araez, C. P. Grey, Current challenges and routes forward for nonaqueous lithium-air batteries. *Chem. Rev.* **120**, 6558–6625 (2020).

5. W.-J. Kwak, Rosy, D. Sharon, C. Xia, H. Kim, L. R. Johnson, P. G. Bruce, L. F. Nazar, Y.-K. Sun, A. A. Frimer, M. Noked, S. A. Freunberger, D. Aurbach, Lithium–oxygen batteries and related systems: Potential, status, and future. *Chem. Rev.* **120**, 6626–6683 (2020).
6. Z. Peng, S. A. Freunberger, L. J. Hardwick, Y. Chen, V. Giordani, F. Bardé, P. Novák, D. Graham, J.-M. Tarascon, P. G. Bruce, Oxygen reactions in a non-aqueous Li^+ electrolyte. *Angew. Chem. Int. Ed.* **50**, 6351–6355 (2011).
7. Y. Zhang, X. Zhang, J. Wang, W. C. McKee, Y. Xu, Z. Peng, Potential-dependent generation of O_2^- and LiO_2 and their critical roles in O_2 reduction to Li_2O_2 in aprotic Li-O_2 batteries. *J. Phys. Chem. C* **120**, 3690–3698 (2016).
8. S. Kang, Y. Mo, S. P. Ong, G. Ceder, A facile mechanism for recharging Li_2O_2 in Li–O_2 batteries. *Chem. Mater.* **25**, 3328–3336 (2013).
9. S. Ganapathy, B. D. Adams, G. Stenou, M. S. Anastasaki, K. Goubitz, X.-F. Miao, L. F. Nazar, M. Wagemaker, Nature of Li_2O_2 oxidation in a Li-O_2 battery revealed by operando X-ray diffraction. *J. Am. Chem. Soc.* **136**, 16335–16344 (2014).
10. Y.-C. Lu, Y. Shao-Horn, Probing the reaction kinetics of the charge reactions of nonaqueous Li-O_2 batteries. *J. Phys. Chem. Lett.* **4**, 93–99 (2013).
11. Y. Wang, Y.-C. Lu, Nonaqueous lithium-oxygen batteries: Reaction mechanism and critical open questions. *Energy Storage Mater.* **28**, 235–246 (2020).
12. R. Cao, E. D. Walter, W. Xu, E. N. Nasybulin, P. Bhattacharya, M. E. Bowden, M. H. Engelhard, J.-G. Zhang, The mechanisms of oxygen reduction and evolution reactions in nonaqueous lithium-oxygen batteries. *ChemSusChem* **7**, 2436–2440 (2014).
13. F. Li, J. Chen, Mechanistic evolution of aprotic lithium-oxygen batteries. *Adv. Energy Mater.* **7**, 1602934 (2017).
14. B. McCloskey, A. Speidel, R. Scheffler, D. C. Miller, V. Viswanathan, J. S. Hummelshøj, J. K. Nørskov, A. C. Luntz, Twin problems of interfacial carbonate formation in nonaqueous Li-O_2 batteries. *J. Phys. Chem. Lett.* **3**, 997–1001 (2012).
15. M. M. Ottakam Thotiyl, S. A. Freunberger, Z. Peng, P. G. Bruce, The carbon electrode in nonaqueous Li–O_2 cells. *J. Am. Chem. Soc.* **135**, 494–500 (2013).
16. X. Yao, Q. Dong, Q. Cheng, D. Wang, Why do lithium-oxygen batteries fail: Parasitic chemical reactions and their synergistic effect. *Angew. Chem. Int. Ed.* **55**, 11344–11353 (2016).
17. L. Johnson, C. Li, Z. Liu, Y. Chen, S. A. Freunberger, P. C. Ashok, B. B. Praveen, K. Dholakia, J.-M. Tarascon, P. G. Bruce, The role of LiO_2 solubility in O_2 reduction in aprotic solvents and its consequences for Li-O_2 batteries. *Nat. Chem.* **6**, 1091–1099 (2014).
18. C. M. Burke, V. Pande, A. Khetan, V. Viswanathan, B. D. McCloskey, Enhancing electrochemical intermediate solvation through electrolyte anion selection to increase nonaqueous Li-O_2 battery capacity. *Proc. Natl. Acad. Sci. U.S.A.* **112**, 9293–9298 (2015).
19. C. Hwang, J. Yoo, G. Y. Jung, S. H. Joo, J. Kim, A. Cha, J.-G. Han, N.-S. Choi, S. J. Kang, S.-Y. Lee, S. K. Kwak, H.-K. Song, Biomimetic superoxide disproportionation catalyst for anti-aging lithium-oxygen batteries. *ACS Nano* **13**, 9190–9197 (2019).
20. I. Landa-Medrano, M. Olivares-Marin, B. Bergner, R. Pinedo, A. Sorrentino, E. Pereiro, I. R. de Larramendi, J. Janek, T. Rojo, D. Tonti, Potassium salts as electrolyte additives in lithium-oxygen batteries. *J. Phys. Chem. C* **121**, 3822–3829 (2017).
21. V. Viswanathan, K. S. Thygesen, J. S. Hummelshøj, J. K. Nørskov, G. Girishkumar, B. D. McCloskey, A. C. Luntz, Electrical conductivity in Li_2O_2 and its role in determining capacity limitations in non-aqueous Li-O_2 batteries. *J. Chem. Phys.* **135**, 214704 (2011).
22. B. D. McCloskey, C. M. Burke, J. E. Nichols, S. E. Renfrew, Mechanistic insights for the development of Li-O_2 battery materials: Addressing Li_2O_2 conductivity limitations and electrolyte and cathode instabilities. *Chem. Commun.* **51**, 12701–12715 (2015).
23. Y. Chen, S. A. Freunberger, Z. Peng, O. Fontaine, P. G. Bruce, Charging a Li-O_2 battery using a redox mediator. *Nat. Chem.* **5**, 489–494 (2013).
24. D. Sun, Y. Shen, W. Zhang, L. Yu, Z. Yi, W. Yin, D. Wang, Y. Huang, J. Wang, D. Wang, J. B. Goodenough, A solution-phase bifunctional catalyst for lithium-oxygen batteries. *J. Am. Chem. Soc.* **136**, 8941–8946 (2014).
25. D. Kundu, R. Black, B. Adams, L. F. Nazar, A highly active low voltage redox mediator for enhanced rechargeability of lithium-oxygen batteries. *ACS Cent. Sci.* **1**, 510–515 (2015).
26. T. Liu, M. Leskes, W. Yu, A. J. Moore, L. Zhou, P. M. Bayley, G. Kim, C. P. Grey, Cycling Li-O_2 batteries via LiOH formation and decomposition. *Science* **350**, 530–533 (2015).
27. W.-J. Kwak, D. Hirshberg, D. Sharon, M. Afri, A. A. Frimer, H.-G. Jung, D. Aurbach, Y.-K. Sun, Li–O_2 cells with LiBr as an electrolyte and a redox mediator. *Energ. Environ. Sci.* **9**, 2334–2345 (2016).
28. S. Matsuda, S. Mori, Y. Kubo, K. Uosaki, K. Hashimoto, S. Nakanishi, Cobalt phthalocyanine analogs as soluble catalysts that improve the charging performance of Li-O_2 batteries. *Chem. Phys. Lett.* **620**, 78–81 (2015).
29. H. D. Lim, H. Song, J. Kim, H. Gwon, Y. Bae, K.-Y. Park, J. Hong, H. Kim, T. Kim, Y. H. Kim, X. Lepró, R. Ovalle-Robles, R. H. Baughman, K. Kang, Superior rechargeability and efficiency of lithium-oxygen batteries: Hierarchical air electrode architecture combined with a soluble catalyst. *Angew. Chem. Int. Ed.* **53**, 3926–3931 (2014).
30. Z. Guo, C. Li, J. Liu, Y. Wang, Y. Xia, A Long-life lithium-air battery in ambient air with a polymer electrolyte containing a redox mediator. *Angew. Chem. Int. Ed.* **56**, 7505–7509 (2017).
31. B. D. Adams, R. Black, Z. Williams, R. Fernandes, M. Cuisinier, E. J. Berg, P. Novak, G. K. Murphy, L. F. Nazar, Towards a stable organic electrolyte for the lithium oxygen battery. *Adv. Energy Mater.* **5**, 1400867 (2015).
32. Z. Peng, S. A. Freunberger, Y. Chen, P. G. Bruce, A reversible and higher-rate Li-O_2 battery. *Science* **337**, 563–566 (2012).
33. B. G. Kim, C. Jo, J. Shin, Y. Mun, J. Lee, J. W. Choi, Ordered mesoporous titanium nitride as a promising carbon-free cathode for aprotic lithium-oxygen batteries. *ACS Nano* **11**, 1736–1746 (2017).
34. W.-B. Luo, T. V. Pham, H.-P. Guo, H.-K. Liu, S.-X. Dou, Three-dimensional array of TiN@Pt_3Cu nanowires as an efficient porous electrode for the lithium-oxygen Battery. *ACS Nano* **11**, 1747–1754 (2017).
35. X. Gao, Y. Chen, L. Johnson, P. G. Bruce, Promoting solution phase discharge in Li-O_2 batteries containing weakly solvating electrolyte solutions. *Nat. Mater.* **15**, 882–888 (2016).
36. W.-H. Ryu, F. S. Gittleson, J. M. Thomsen, J. Li, M. J. Schwab, G. W. Brudvig, A. D. Taylor, Heme biomolecule as redox mediator and oxygen shuttle for efficient charging of lithium-oxygen batteries. *Nat. Commun.* **7**, 12925 (2016).
37. J. Zhang, B. Sun, Y. Zhao, A. Tkacheva, Z. Liu, K. Yan, X. Guo, A. M. McDonagh, D. Shanmukaraj, C. Wang, T. Rojo, M. Armand, Z. Peng, G. Wang, A versatile functionalized ionic liquid to boost the solution-mediated performances of lithium-oxygen batteries. *Nat. Commun.* **10**, 602 (2019).
38. Y. Zhang, L. Wang, X. Zhang, L. Guo, Y. Wang, Z. Peng, High-capacity and high-rate discharging of a coenzyme Q10-catalyzed Li-O_2 battery. *Adv. Mater.* **30**, 1705571 (2018).
39. B. J. Bergner, A. Schürmann, K. Peppler, A. Garsuch, J. Janek, TEMPO: A mobile catalyst for rechargeable Li-O_2 batteries. *J. Am. Chem. Soc.* **136**, 15054–15064 (2014).
40. B. G. Kim, S. Kim, H. Lee, J. W. Choi, Wisdom from the human eye: A synthetic melanin radical scavenger for improved cycle life of Li–O_2 battery. *Chem. Mater.* **26**, 4757–4764 (2014).
41. Z. Liang, Q. Zou, J. Xie, Y.-C. Lu, Suppressing singlet oxygen generation in lithium-oxygen batteries with redox mediators. *Energ. Environ. Sci.* **13**, 2870–2877 (2020).
42. A. S. Jalilov, L. G. Nilewski, V. Berka, C. Zhang, A. A. Yakovenko, G. Wu, T. A. Kent, A.-L. Tsai, J. M. Tour, Perylene diimide as a precise graphene-like superoxide dismutase mimetic. *ACS Nano* **11**, 2024–2032 (2017).
43. S. Nakatsuji, K. Aoki, H. Akutsu, J.-i. Yamada, T. Kojima, J.-i. Nishida, Y. Yamashita, Spin-carrying naphthalenediimide and perylenediimide derivatives. *Bull. Chem. Soc. Jpn* **83**, 1079–1085 (2010).
44. M. T. Colvin, E. M. Giacobbe, B. Cohen, T. Miura, A. M. Scott, M. R. Wasielewski, Competitive electron transfer and enhanced intersystem crossing in photoexcited covalent TEMPO-perylene-3, 4: 9, 10-bis (dicarboximide) dyads: Unusual spin polarization resulting from the radical-triplet interaction. *J. Phys. Chem. A* **114**, 1741–1748 (2010).
45. N. Mahne, B. Schafzahl, C. Leypold, M. Leypold, S. Grumm, A. Leitgeb, G. A. Strohmeier, M. Wilkening, O. Fontaine, D. Kramer, C. Slugovc, S. M. Borisov, S. A. Freunberger, Singlet oxygen generation as a major cause for parasitic reactions during cycling of aprotic lithium-oxygen batteries. *Nat. Energy* **2**, 17036 (2017).
46. E. Mourad, Y. K. Petit, R. Spezia, A. Samojlov, F. F. Summa, C. Prehal, C. Leypold, N. Mahne, C. Slugovc, O. Fontaine, S. Brutti, S. A. Freunberger, Singlet oxygen from cation driven superoxide disproportionation and consequences for aprotic metal–O_2 batteries. *Energ. Environ. Sci.* **12**, 2559–2568 (2019).
47. A. Datar, K. Balakrishnan, L. Zang, One-dimensional self-assembly of a water soluble perylene diimide molecule by pH triggered hydrogelation. *Chem. Commun.* **49**, 6894–6896 (2013).
48. J. Zhang, B. Sun, X. Xie, Y. Zhao, G. Wang, A bifunctional organic redox catalyst for rechargeable lithium-oxygen batteries with enhanced performances. *Adv. Sci.* **3**, 1500285 (2016).
49. W. Guo, Y.-X. Yin, S. Xin, Y.-G. Guo, L.-J. Wan, Superior radical polymer cathode material with a two-electron process redox reaction promoted by graphene. *Energ. Environ. Sci.* **5**, 5221–5225 (2012).
50. D. Wu, G. Zhang, D. Lu, L. Ma, Z. Xu, X. Xi, R. Liu, P. Liu, Y. Su, Perylene diimide-diamine/carbon black composites as high performance lithium/sodium ion battery cathodes. *J. Mater. Chem. A* **6**, 13613–13618 (2018).
51. R. Black, A. Shyamsunder, P. Adeli, D. Kundu, G. K. Murphy, L. F. Nazar, The Nature and impact of side reactions in glyme-based sodium-oxygen batteries. *ChemSusChem* **9**, 1795–1803 (2016).
52. N. B. Aetukuri, B. D. McCloskey, J. M. García, L. E. Krupp, V. Viswanathan, A. C. Luntz, Solvating additives drive solution-mediated electrochemistry and enhance toroid growth in non-aqueous Li-O_2 batteries. *Nat. Chem.* **7**, 50–56 (2015).
53. D. Aurbach, B. D. McCloskey, L. F. Nazar, P. G. Bruce, Advances in understanding mechanisms underpinning lithium-air batteries. *Nat. Energy* **1**, 16128 (2016).
54. Y. Zhang, Q. Cui, X. Zhang, W. C. McKee, Y. Xu, S. Ling, H. Li, G. Zhong, Y. Yang, Z. Peng, Amorphous Li_2O_2: Chemical synthesis and electrochemical properties. *Angew. Chem. Int. Ed.* **55**, 10717–10721 (2016).

55. Y. Zhao, J. Zhang, W. Wu, X. Guo, P. Xiong, H. Liu, G. Wang, Cobalt-doped MnO_2 ultrathin nanosheets with abundant oxygen vacancies supported on functionalized carbon nanofibers for efficient oxygen evolution. *Nano Energy* **54**, 129–137 (2018).
56. Y. Wang, N.-C. Lai, Y.-R. Lu, Y. Zhou, C.-L. Dong, Y.-C. Lu, A solvent-controlled oxidation mechanism of Li_2O_2 in lithium-oxygen batteries. *Joule* **2**, 2364–2380 (2018).
57. Y. K. Petit, E. Mourad, C. Prehal, C. Leypold, A. Windischbacher, D. Mijailovic, C. Slugovc, S. M. Borisov, E. Zojer, S. Brutti, O. Fontaine, S. A. Freunberger, Mechanism of mediated alkali peroxide oxidation and triplet versus singlet oxygen formation. *Nat. Chem.* **13**, 465–471 (2021).
58. Z. Liang, Y. Zhou, Y.-C. Lu, Dynamic oxygen shield eliminates cathode degradation in lithium-oxygen batteries. *Energ. Environ. Sci.* **11**, 3500–3510 (2018).
59. B. Sun, X. Huang, S. Chen, P. Munroe, G. Wang, Porous graphene nanoarchitectures: An efficient catalyst for low charge-overpotential, long life, and high capacity lithium–oxygen batteries. *Nano Lett.* **14**, 3145–3152 (2014).
60. H.-D. Lim, B. Lee, Y. Zheng, J. Hong, J. Kim, H. Gwon, Y. Ko, M. Lee, K. Cho, K. Kang, Rational design of redox mediators for advanced Li-O_2 batteries. *Nat. Energy* **1**, 16066 (2016).

Acknowledgments: We acknowledge Y. Chen and C. Tan from Nanjing Tech University, Nanjing, for valuable discussions of in situ DEMS. **Funding:** This project was financially supported by the Australian Research Council (ARC) through the ARC Discovery Project (DP160104340, DP170100436, DP180102297, and DP200101249) and ARC Discovery Early Career Researcher Award (DE180100036). Z.P. was credited to National Key R&D Program of China (project nos. 2016YFB0100100 and 2018YFB0104400), National Natural Science Foundation of China (21972055, 21825202, 21575135, 21733012, and 21972133), and the Newton Advanced Fellowships (NAF/R2/180603). The work at Argonne National Laboratory was supported by the U.S. Department of Energy (DOE), Office of Energy Efficiency and Renewable Energy, Vehicle Technologies Office. Argonne National Laboratory was operated for the DOE Office of Science by UChicago Argonne LLC under contract no. DE-AC02-06CH11357. **Author contributions:** J.Z., Y.Z., and G.W. conceived the idea. J.Z., A.T., and Y.X. synthesized the PDI-TEMPO molecules. J.Z. and Y.Z. performed the electrochemical experiments. J.Z. and K.Y. performed experiments on lithium anode stability tests. J.Z., and Y.Z. performed EPR measurement. J.Z., Y.Z., S.W., X.G., and F.Q. conducted characterizations. B.S., A.M.M., P.H., H.Z., Z.P., and J.L. were all involved in the discussions. All the authors contributed to the writing of the manuscript before submission. **Competing interests:** The authors declare that they have no competing interests. **Data and materials availability:** All data needed to evaluate the conclusions in the paper are present in the paper and/or the Supplementary Materials.

Submitted 2 September 2021
Accepted 26 November 2021
Published 21 January 2022
10.1126/sciadv.abm1899

ScienceAdvances

A long-life lithium-oxygen battery via a molecular quenching/mediating mechanism

Jinqiang Zhang, Yufei Zhao, Bing Sun, Yuan Xie, Anastasia Tkacheva, Feilong Qiu, Ping He, Haoshen Zhou, Kang Yan, Xin Guo, Shijian Wang, Andrew M. McDonagh, Zhangquan Peng, Jun Lu, and Guoxiu Wang

Sci. Adv., **8** (3), eabm1899.
DOI: 10.1126/sciadv.abm1899

Science Advances (ISSN) is published by the American Association for the Advancement of Science. 1200 New York Avenue NW, Washington, DC 20005. The title *Science Advances* is a registered trademark of AAAS.